Calculation of the Flow Around the A-airfoil Using an Incompressible Code Based on SIMPLEC and a Two-Layer $k - \varepsilon$ Model

L. Davidson
CERFACS
42, Av. Gustave Coriolis
31057 Toulouse
FRANCE
Report TR/RF/92/73, 1992

Summary

In the Computational Aerodynamic Group at *CERFACS* work has been going on since 1988 on calculating the flow around high-lift two-dimensional airfoils with the objective to be able to predict stall. The flow conditions of the case are $R_e = 2.1 \times 10^6, M = 0.15$ and angles of attack from zero to 19 deg. Work has been carried out improving the numerical scheme [9], as well as implementing and testing different turbulence models such as the Baldwin-Lomax model, and various $k - \varepsilon$ models [1, 5]. The main drawback in these efforts was that the separation zone near the trailing edge was much under-predicted compared with experiments, and when the angle of attack was increased the predicted lift coefficient increased even though the experiments show that stall should occur. It was believed that this failure of predicting stall could be due to inadequate turbulence models, and therefore a two-layer ASM was implemented [6, 8]. With this turbulence model stall was predicted.

In all works cited above, an explicit Runge-Kutta code was used. In the present work an incompressible SIMPLEC code is used in order to verify that the results obtained with the Runge-Kutta code are not code-dependent.

Acknowledgements

This work has been carried out during a visit of CERFACS in April, 1992, and it is a part of a collaboration project between NSC (National Supercomputing Center) in Sweden and CERFACS. Financial support from NSC and NUTEK is greatfully acknowledged.

In this project the flow around the A-airfoil is going to be computed with two completely different codes: an incompressible SIMPLEC code and a compressible MacGormack code. The persons involved in the project are – apart from the author – A. KOURTA and S. UNDREINER, CERFACS.

1 Equations

1.1 General Transport Equation

The general transport equation in Cartesian coordinates for a variable Φ is

$$\frac{\partial}{\partial x_m}\left(\rho U_m \Phi\right) = \frac{\partial}{\partial x_m}\left(\Gamma_\Phi \frac{\partial \Phi}{\partial x_m}\right) + \overline{S}^\Phi, \tag{1}$$

where $\overline{S}^\Phi$ denotes the source per unit volume for the variable Φ. The flux vector J_m, containing convection and diffusion terms are defined as follows

$$J_m = \rho U_m \Phi - \Gamma_\Phi \frac{\partial \Phi}{\partial x_m}. \tag{2}$$

Substituting Eq. (2) in Eq. (1), we get

$$\frac{\partial J_m}{\partial x_m} = \overline{S}^\Phi.$$

Or in vector notation, we have

$$\nabla \cdot \mathbf{J} = \overline{S}^\Phi.$$

Integrating the above equation over a typical control volume with volume V and surface area A, and using the Gauss' law we get

$$\int_A \mathbf{J} \cdot \mathbf{dA} = \int_V \overline{S}^\Phi dV. \tag{3}$$

1.2 Mean Flow Equations

We have the continuity equation

$$\frac{\partial}{\partial x_i}\left(\rho U_i\right) = 0. \tag{4}$$

The momentum equation is expressed as

$$\frac{\partial}{\partial x_j}\left(\rho U_i U_j\right) = -\frac{\partial p}{\partial x_i} + \frac{\partial}{\partial x_j}\left(\mu_{eff}\frac{\partial U_i}{\partial x_j}\right). \tag{5}$$

1.3 Turbulence Model

The standard $k-\varepsilon$ turbulence model is used. The transport equations for k and ε can be written in tensor notation as

$$\frac{\partial}{\partial x_j}\left(\rho U_j k\right) = \frac{\partial}{\partial x_j}\left(\frac{\mu_{eff}}{\sigma_k}\frac{\partial k}{\partial x_j}\right) + P_k - \rho\varepsilon \tag{6}$$

$$\frac{\partial}{\partial x_j}\left(\rho U_j \varepsilon\right) = \frac{\partial}{\partial x_j}\left(\frac{\mu_{eff}}{\sigma_\varepsilon}\frac{\partial \varepsilon}{\partial x_j}\right) + c_{\varepsilon 1}\frac{\varepsilon}{k}\left(P_k - c_{\varepsilon 2}\rho\varepsilon\right). \tag{7}$$

The generation term P_k can be expressed in tensor notation as

$$P_k = \mu_t \frac{\partial U_i}{\partial x_j}\left(\frac{\partial U_i}{\partial x_j} + \frac{\partial U_j}{\partial x_i}\right), \tag{8}$$

The turbulent viscosity μ_t is calculated as

$$\mu_t = \rho c_\mu \frac{k^2}{\varepsilon}.$$

The effective viscosity $\mu_{\mathbf{eff}}$ is obtained as

$$\mu_{\mathbf{eff}} = \mu + \mu_t.$$

1.4 Near-Wall Treatment

Near the walls the one-equation model by Wolfshtein [16], modified by Chen and Patel [4], is used. In this model the standard k equation is solved. The turbulent length scales are prescribed as:

$$\ell_\mu = c_\ell n\left[1 - exp\left(-R_n/A_\mu\right)\right], \quad \ell_\varepsilon = c_\ell n\left[1 - exp\left(-R_n/A_\varepsilon\right)\right]$$

(n is the normal distance from the wall) so that the dissipation term in the k-equation and the turbulent viscosity are obtained as:

$$\varepsilon = \frac{k^{3/2}}{\ell_\varepsilon}, \quad \mu_t = c_\mu \rho\sqrt{k}\ell_\mu \tag{9}$$

The Reynolds number R_n and the constants are defined as

$$R_n = \frac{\sqrt{k}n}{\nu},\ c_\mu = 0.09,\ \ c_\ell = \kappa c_\mu^{-3/4},\ \ A_\mu = 70,\ \ A_\varepsilon = 2c_\ell$$

The one-equation model is used near the walls (for $R_n \leq 250$; the matching line is chosen along a pre-selected grid line), and the standard k and ε-equations in the remaining part of the flow.

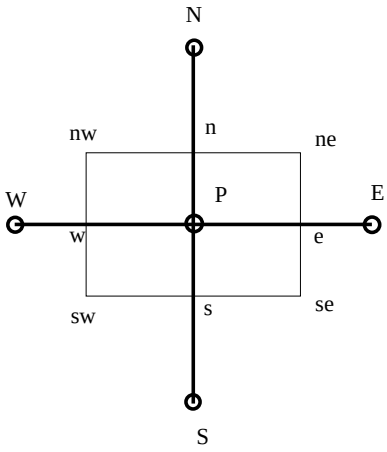

Figure 1: *Control volume and notation (for clarity Fig. 2 is drawn in Cartesian coordinate system).*

2 The Code

2.1 Basis

In this section the CALC-BFC code developed by Davidson and Farhanieh [7], is presented. CALC-BFC (**B**oundary **F**itted **C**oordinates) is a general-purpose computer code for three-dimensional complex geometries. The program uses Cartesian velocity components. In most finite volume programs staggered grids for the velocities have been used [13]. In the present work collocated variables are used, which means that velocities are stored along with all scalar variables like p, k, ε at the centre of the contol volume. This concept was suggested by Rhie and Chow [14].

Equation 3 is discretized using standard control volume formulation as described by Patankar [13]. Integrating Eq. 3 over a control volume (See Fig 2) yields

$$(\mathbf{J}\cdot\mathbf{A})_e + (\mathbf{J}\cdot\mathbf{A})_w + (\mathbf{J}\cdot\mathbf{A})_n + (\mathbf{J}\cdot\mathbf{A})_s + (\mathbf{J}\cdot\mathbf{A})_h + (\mathbf{J}\cdot\mathbf{A})_\ell = S^\Phi \delta V.$$

Note that the positive signs on the terms containing contributions from west and south surfaces will be negative because the scalar products in themselves are negative.

The discretized equation will be of the form

$$a_P \Phi_P = \sum_{nb} a_{nb}\Phi_{nb} + S_C^\Phi, \tag{10}$$

where

$$a_P = \sum a_{nb} - S_P^{\Phi}.$$

The coefficients a_{nb} contain the contributions due to both convection and diffusion. The source terms S_C^{Φ} and S_P^{Φ} contain the remaining terms.

2.2 Convection

The convection which is the first part of the flux vector **J** (Eq. 2), is the scalar product of the velocity vector and the area vector multiplied by the density. For north face we obtain (see Fig. 3)

$$\dot{m}_n = (\rho \mathbf{u} \cdot \mathbf{A})_n = \rho_n \left(U_n A_{nx} + V_n A_{ny} + W_n A_{nz} \right).$$

Since the Cartesian areas A_{nx}, A_{ny}, A_{nz} are stored in the program, the calculation of the convective contributions to **J** is straight-forward. Special care must however be taken when the velocities are interpolated from their storage location at the cell center to the control volume faces to avoid non physical oscillations. Rhie and Chow [14] solved this problem. Below is described how the velocities at control volume faces are calculated. For simplicity Cartesian coordinates are used.

When the pressure gradient is added to the momentum equation standard linear interpolation is used, i.e.,

$$\left(\frac{\partial p}{\partial y} \right) = \frac{p_n - p_s}{|\mathbf{sn}|},$$

where

$$p_n = f_y p_N + (1 - f_y)\, p_P.$$

For example, when calculating the velocity at the north face the pressure gradient is subtracted so that

$$V_P^{\#} = V_P - \frac{-\left(p_n - p_s\right) \delta V}{|\mathbf{sn}| \left(a_P\right)_P},$$

and

$$V_N^{\#} = V_N - \frac{-\left(p_{Nn} - p_n\right)\delta V}{\left|\mathbf{n}\left(\mathbf{Nn}\right)\right|\left(a_P\right)_N},$$

where a_P is the discretized coefficient in the V-momentum equations (see Eq. 10). The V-velocity at the north face of the control volume is now calculated as

$$V_n = f_y V_N^{\#} + \left(1 - f_y\right) V_P^{\#} - \frac{\left(p_N - p_P\right)\delta V}{\left|\mathbf{PN}\right|\left(a_P\right)_n}.$$

The advantage of the previous expression is obvious, i.e., the pressure gradient is calculated using the adjacent nodes of face n. This prevents non physical oscillations in the pressure field.

Three different differencing schemes for the convective terms in the momentum equations are tested:

- the second-order van Leer scheme [11];
- the QUICK scheme of Leonard [12], which is a third-order accurate scheme
- the first-order hybrid central/upwind scheme [13].

For the convective terms in the k and ε-equations, the hybrid upwind/central differencing scheme is used.

2.3 Diffusion

Diffusion is the second part of the flux vector $\mathbf{J}$ in Eq. 2, and it has the form

$$\mathcal{D} = \left(\mathbf{J}\cdot\mathbf{A}\right)_{diff} = -\Gamma_\Phi \mathbf{A}\cdot\nabla\Phi.$$

For example, the Cartesian coordinates (x, y, z) for the north face are given by,

$$-\left\{\Gamma_\Phi \mathbf{A}\cdot\nabla\Phi\right\}_n = -\left\{\Gamma_\Phi\left(A_x\frac{\partial\Phi}{\partial x} + A_y\frac{\partial\Phi}{\partial y} + A_z\frac{\partial\Phi}{\partial z}\right)\right\}_n,$$

and in curvilinear coordinates (ξ, η, ζ)

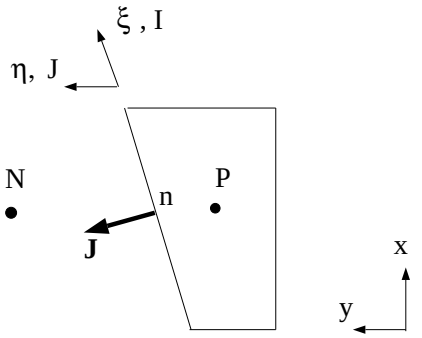

Figure 2: *The flux through the north face of a non-orthogonal control volume. ξ is along the I-grid lines, and η is along the J-grid lines.*

$$-\{\mathbf{A}\cdot\nabla\Phi\}_n = -\left\{\mathbf{A}\cdot\mathbf{g}_i g^{ij}\frac{\partial\Phi}{\partial\xi_j}\right\}_n = -\left\{|\mathbf{A}|\mathbf{n}\cdot\mathbf{g}_i g^{ij}\frac{\partial\Phi}{\xi_j}\right\}_n .$$

The covariant (tangential) base vectors $\mathbf{g}_1, \mathbf{g}_2$ and $\mathbf{g}_3$ correspond to I, J and K grid lines respectively. The metric tensor is involved because the components of the product $\mathbf{A}\cdot\mathbf{g}_i$ and the derivative $\partial\Phi/\partial\xi_j$ are both covariant, and the product of their (contravariant) base vectors is not equal to zero or one (as in Cartesian coordinate systems) since they are non-orthogonal to each other.

The diffusive terms are discretized using central differencing, which is of second order accuracy [13].

2.4 Pressure Correction Equation

The discretized continuity equation in one dimension takes the form

$$\dot{m}_n - \dot{m}_s = 0. \tag{11}$$

where $\dot{m}$ denotes the mass flux, which is calculated as

$$\dot{m} = \rho\mathbf{A}\cdot\mathbf{u}.$$

In SIMPLEC [13] the mass flux is divided into two parts namely (a) old value $\dot{m}^*$ and (b) correction $\dot{m}'$ to $\dot{m}^*$, so that

$$\dot{m} = \dot{m}^* + \dot{m}'.$$

The covariant velocity components are in SIMPLEC related to the pressure gradient as

$$V_i = -\frac{\delta V}{a_P}\frac{\partial p}{\partial x_i}, \tag{12}$$

where a_P is obtained from the discretized U_i-equation (see Eq. 10). The mass flux correction at the north face can now be written as

$$\dot{m}'_n = \rho_n \mathbf{A} \cdot \mathbf{u}' = \rho \left(A_{nx}u'_n + A_{ny}v'_n + A_{nz}w'_n\right) = \left(\rho \mathbf{A} \cdot \mathbf{g}^j V'_j\right)_n.$$

Using Eq. 12 we get

$$\dot{m}'_n = \left\{\rho \mathbf{A} \cdot \left(-\frac{\delta V}{a_P}\frac{\partial p'}{\partial x_j}\mathbf{g}^j\right)\right\}_n = -\left(\frac{\delta V \rho}{a_P}\mathbf{A} \cdot \nabla p'\right)_n = 0, \tag{13}$$

where p' is the pressure correction. From Eqs. 11 and 13 we obtain

$$\left(\frac{\delta V \rho}{a_P}\mathbf{A} \cdot \nabla p'\right)_s - \left(\frac{\delta V \rho}{a_P}\mathbf{A} \cdot \nabla p'\right)_n + \dot{m}^*_n - \dot{m}^*_s = 0.$$

This equation is a diffusion equation for the pressure correction p'.

3 Boundary Conditions

3.1 Far field

U and V are precribed from the Reynolds number. The speed at the far field is set to one, and thus

$$U = \cos\alpha, \quad V = \sin\alpha$$

where α is the angle of incidence.

The turbulent quantities are set to small values ($k = \varepsilon = 1 \times 10^{-20}$). No boundary condition is required for the pressure.

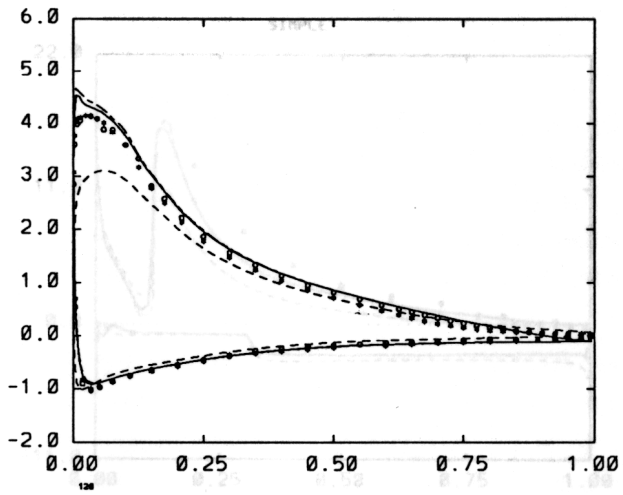

Figure 3: *Comparison between calculated and experimental surface pressure.* $\alpha = 13.3^o$. *——, predictions using van Leer scheme;* $- - - - - -$*, predictions using hybrid scheme; — - — -, predictions using the QUICK scheme; markers, experiments (o: F1 windtunnel;* $*$*: F2 windtunnel).*

3.2 Walls

U, V and k are set to zero. Transition is imposed by setting k and ε close to zero before the transition point ($x_{tr} = 0.12$ on the suction side, and $x_{tr} = 0.3$ on the pressure side).

4 Results

A C-mesh with 176×32, generated by Chanez and Palicot [3], has been used. The near-wall nodes are located at $y^+ \simeq 2$, and 3 to 5 nodes – in the normal direction – are situated in the region $0 \leq y^+ \leq 20$.

The calculated results are compared with experimental data taken from [2, 10]. The Reynolds number and the Mach number are 2.1×10^6 and 0.15, respectively. Measurements have been carried out in two windtunnels, F1 and F2. In the F1 windtunnel, global characteristics such as friction coefficients and surface pressures were measured. The flow field was studied more in detail in the F2 windtunnel, where mean velocity profiles and Reynolds stresses were measured using a three component LDV-system. The blockage effect in the F2 tunnel was more important than in the F1 tunnel, leading to three-dimensional effects for $\alpha \geq 13^o$.

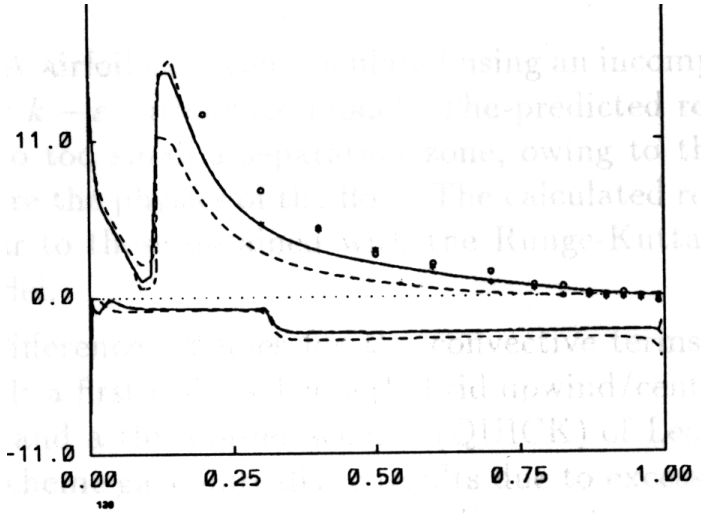

Figure 4: *Comparison between calculated and experimental skin friction.* $\alpha = 13.3^o$. ——, *predictions using van Leer scheme;* − − − − − −, *predictions using hybrid scheme;* — - — -, *predictions using the QUICK scheme; markers, experiments (o: F1 windtunnel;* $*$*: F2 windtunnel).*

The main characteristics of the flow are presented in form of c_p and c_F-curves in Figs. 3 and 4. Three different differencing schemes have been used for the mean flow equations: the second-order scheme of van Leer [11], the third-order scheme QUICK of Leonard [12], and the first-order hybrid central/upwind scheme [13]. The difference between the first-order scheme and the two other schemes is dramatic. This is also relected in the lift coefficients, see Table 1.

The c_L predicted with the QUICK scheme is slightly higher than that using the van Leer scheme, which is reflected in the c_P-curve, where the suctions peak is slightly higher for the QUICK scheme than for the van Leer scheme.

	c_L
Experiments in F1	1.55
Experiments in F2	1.49
predictions, van Leer	1.59
predictions, QUICK	1.60
predictions, hybrid	1.28

Table 1: Comparison of calculated lift coefficients with experiments.

The predictions results are close to those obtained with the Runge-Kutta code [5].

5 Conclusions

The flow around the A-airfoil has been calculated using an incompressible SIMPLEC code and a two-layer $k-\varepsilon$ turbulence model. The predicted results give too high lift coefficients due to too small a separation zone, owing to the deficiency of the $k-\varepsilon$ model to capture the physics of the flow. The calculated results in the present work are very similar to those obtained with the Runge-Kutta code [5] using the same turbulence model.

Three different difference schemes for the convective terms in the momentum equations were tested: a first-order scheme (hybrid upwind/central), a second-order scheme of van Leer, and a third-order scheme (QUICK) of Leonard. It was found that the first-order scheme gave unrealistic results due to excessive numerical diffusion, where the other two schemes gave very similar results.

References

[1] de CAMBRAY, E. – Evaluation d'un modèle $k-\varepsilon$ dans un code Navier-Stokes, Thèse DEA, CERFACS, September, 1990.

[2] CAPBERN, C. and BONNET, C. – Opération décrochage: Rapport Final de Synthèse, Rapport Aerospatiale 443.535./89, Toulouse, 1989.

[3] CHANEZ, Ph. and PALICOT, L. – Évaluation d'un code Navier-Stokes bidimensionnnel pour le calcul de l'écoulement autour d'un profil d'aile, Note interne Aerospatiale, 443.548/90, 1990

[4] CHEN, H.C. and PATEL, V.C. – Practical Near-Wall Turbulence Models for Complex Flows Including Separation, AIAA Paper No 87-1300, Honolulu, June 1987.

[5] DAVIDSON, L. – Task 2.1 – Maximum Lift for Single Element-Airfoil, Brite-Euram/Euroval, Final report, 1991.

[6] DAVIDSON, L. – Calculation of the Flow Around a High-Lift Airfoil Using an Explicit Code and an Algebraic Reynolds Stress Model, Proc. Seventh Int. Conf. on Numerical Methods in Laminar and Turbulent Flow, Vol. 7, Part 2, pp. 852-862, Stanford, 1991.

[7] DAVIDSON, L. and FARHANIEH, B. – CALC-BFC: A Finite-Volume Code Employing Collocated Variable Arrangement and Cartesian Velocity Components for Computation of Fluid Flow and Heat Transfer in Complex Three-Dimensional Geometries, Rept., Dept. of Applied Thermodynamics and Fluid Mechanics, Chalmers University of Technology, Gothenburg, Sweden, 1991.

[8] DAVIDSON, L. and RIZZI, A. – Navier-Stokes Computation of Airfoil in Stall Using Algebraic Reynolds-Stress Model, AIAA-paper 92-0195, Reno, 1992.

[9] GENDRE, P. – Computation of Low Speed Flow Around High-Lift Single Element Airfoils With a 2D Navier-Stokes Solver, Proc. Second World Congress on Computational Mechanics, extended abstracts, pp. 202-205, Stuttgart, 1990.

[10] GLEYZES, C. – Opération décrochage: Résultats de la deuxième campagne d'essais à F2 (mesures de pression et vélocimetrie laser), Rapport Final ONERA/CERT 57/5004.22, Toulouse, 1989.

[11] van LEER, B. – Towards the Ultimate Conservative Difference Scheme. II. Monotonicity and Conservation Combined in a Second-Order Scheme, *J. Comp. Phys.*, **14**, 361-370, 1974.

[12] LEONARD, B. – A Stable and Accurate Convective Modelling Procedure Based on Quadratic Upstream Interpolation, *Comp. Meth. Appl. Mech. Engng.*, **19**, 59-98, 1979.

[13] PATANKAR, S.V. – Numerical Heat Transfer and Fluid Flow, McGraw-Hill, Washington, 1980.

[14] RHIE, C.M. and CHOW, W.L. – Numerical Study of the Turbulent Flow Past an Airfoil With Trailing Edge Separation, *AIAA J.*, **21**, pp. 1525-1532, 1983.

[15] RODI, W. – Turbulence Models and Their Applications in Hydraulics, International Association of Hydraulics Research, Monograph, Delft, 1980.

[16] WOLFSHTEIN, M. – The Velocity and Temperature Distribution in One-Dimensional Flow with Turbulence Augmentation and Pressure Gradient, *Int. J. Mass Heat Transfer*, **12**, pp. 301-318, 1969.